Imidazo[4,5-*f*]-1,10-phenanthrolines: Versatile Ligands for the Design of Metallomesogens

Thomas Cardinaels,*[,†] Jan Ramaekers,[†] Peter Nockemann,[†] Kris Driesen,[†] Kristof Van Hecke,[†] Luc Van Meervelt,[†] Shengbin Lei,[†] Steven De Feyter,[†] Daniel Guillon,[‡] Bertrand Donnio,*[,‡] and Koen Binnemans[‡]

Department of Chemistry, Katholieke Universiteit Leuven, Celestijnenlaan 200F, B-3001 Leuven, Belgium, and Institut de Physique et Chimie des Matériaux de Strasbourg, UMR 7504 CNRS-Université Louis Pasteur, BP43, 23 rue du Loess, F-67034 Strasbourg Cedex 2, France

Received March 7, 2007. Revised Manuscript Received July 20, 2007

2-Aryl-substituted imidazo[4,5-*f*]-1,10-phenanthrolines were used as building blocks for metal-containing liquid crystals (metallomesogens). Imidazo[4,5-*f*]-1,10-phenanthrolines are versatile ligands because they can form stable complexes with various d-block transition metals, including platinum(II) and rhenium(I), as well as with lanthanide(III) and uranyl ions and they can easily be structurally modified by a judicious choice of benzaldehyde precursor. None of the ligands designed for this study were liquid-crystalline. However, mesomorphism could be induced by their coordination to various metallic fragments. The thermal behavior of the metal complexes depended on the metal-to-ligand ratio and the substitution pattern of the coordinating ligands. Complexes with a metal-to-ligand ratio of 1:1 [ML, with M = Pt(II), Re(I)] were not liquid-crystalline. The lanthanide(III) complexes with a metal-to-ligand ratio of 1:2 [ML_2, with M = Ln(III)] formed an enantiotropic cubic mesophase or were not liquid-crystalline, depending on the nature of the lanthanide(III) ion and the substitution pattern of the ligands. A 1:3 uranyl complex of the type $[ML_3]^{2+}$ exhibited a hexagonal columnar mesophase over a broad temperature range. Self-assembled monolayers of a europium(III) complex were investigated by scanning tunneling microscopy, which revealed that the complex formed well-ordered structures over long distances at the 1-octanoic acid−graphite interface. The rhenium(I) complexes and the europium(III) complexes with 2-thenoyltrifluoroacetonate or dibenzoylmethanate and imidazo[4,5-*f*]-1,10-phenanthroline showed good luminescence properties.

Introduction

The rationale for incorporation of transition metals into liquid crystals is the opportunity to combine the properties of liquid crystals (which are anisotropic fluids) with the unique properties of d-block and f-block transition metals (e.g., their magnetic and photophysical properties and redox behavior).[1–4] The design of metal-containing liquid crystals (*metallomesogens*) is a challenge, because the presence of a metal center often modifies the mesomorphic behavior of the free ligand (e.g., by stabilization, modification, or suppression of existing mesophases of the ligand or induction of new mesophases).[5,6] On the other hand, transition metals aid in the construction of mesogenic materials with original molecular architectures that cannot be obtained by the use of pure organic systems. Examples are lanthanide(III) complexes,[7–11] gold metallacrowns,[12] macrocyclic azacrown complexes,[13–15] and long-chain carboxylate metal salts.[3,16] Additionally, the radius of the metal ion can influence the

* To whom correspondence should be addressed. E-mail: thomas.cardinaels@chem.kuleuven.be, bdonnio@ipcms.u-strasbg.fr.
† Katholieke Universiteit Leuven.
‡ CNRS-Université Louis Pasteur.

(1) *Metallomesogens: Synthesis, Properties, and Applications*; Serrano, J. L., Ed.; VCH: Weinheim, Germany, 1996.
(2) Binnemans, K.; Görller-Walrand, C. *Chem. Rev.* **2002**, *102*, 2303–2345.
(3) Donnio, B.; Guillon, D.; Deschenaux, R.; Bruce, D. W. Metallomesogens. In *Comprehensive Coordination Chemistry II*; McCleverty, J. A., Meyer, T. J., Eds.; Elsevier: Oxford, U.K., 2003; pp 357–627.
(4) Piguet, C.; Bünzli, J. C. G.; Donnio, B.; Guillon, D. *Chem. Commun.* **2006**, 3755–3768.
(5) Bruce, D. W. *Adv. Mater.* **1994**, *6*, 699–701.
(6) Terazzi, E.; Suarez, S.; Torelli, S.; Nozary, H.; Imbert, D.; Mamula, O.; Rivera, J. P.; Guillet, E.; Benech, J. M.; Bernardinelli, G.; Scopelliti, R.; Donnio, B.; Guillon, D.; Bünzli, J. C. G.; Piguet, C. *Adv. Funct. Mater.* **2006**, *16*, 157–168.
(7) Binnemans, K.; Galyametdinov, Y. G.; Collinson, S. R.; Bruce, D. W. *J. Mater. Chem.* **1998**, *8*, 1551–1553.
(8) Binnemans, K.; Galyametdinov, Y. G.; Van Deun, R.; Bruce, D. W.; Collinson, S. R.; Polishchuk, A. P.; Bikchantaev, I.; Haase, W.; Prosvirin, A. V.; Tinchurina, L.; Litvinov, I.; Gubajdullin, A.; Rakhmatullin, A.; Uytterhoeven, K.; Van Meervelt, L. *J. Am. Chem. Soc.* **2000**, *122*, 4335–4344.
(9) Galyametdinov, Y. G.; Athanassopoulou, M. A.; Griesar, K.; Kharitonova, O.; Bustamante, E. A. S.; Tinchurina, L.; Ovchinnikov, I. V.; Haase, W. *Chem. Mater.* **1996**, *8*, 922–926.
(10) Galyametdinov, Y. G.; Haase, W.; Malykhina, L. V.; Prosvirin, A. V.; Bikchantaev, I.; Rakhmatullin, A.; Binnemans, K. *Chem.—Eur. J.* **2001**, *7*, 99–105.
(11) Nozary, H.; Torelli, S.; Guenee, L.; Terazzi, E.; Bernardinelli, G.; Donnio, B.; Guillon, D.; Piguet, C. *Inorg. Chem.* **2006**, *45*, 2989–3003.
(12) Barbera, J.; Elduque, A.; Gimenez, R.; Lahoz, F. J.; Lopez, J. A.; Oro, L. A.; Serrano, J. L. *Inorg. Chem.* **1998**, *37*, 2960–2967.
(13) Lattermann, G.; Schmidt, S.; Kleppinger, R.; Wendorff, J. H. *Adv. Mater.* **1992**, *4*, 30–33.
(14) Neve, F.; Ghedini, M.; Demunno, G.; Levelut, A. M. *Chem. Mater.* **1995**, *7*, 688–693.
(15) Schmidt, S.; Lattermann, G.; Kleppinger, R.; Wendorff, J. H. *Liq. Cryst.* **1994**, *16*, 693–702.
(16) Binnemans, K. *Chem. Rev.* **2005**, *105*, 4148–4204.

10.1021/cm070637i CCC: $40.75
Published on Web 01/23/2008

transition temperatures and even the type of mesophase. This effect has been studied in mesogens of trivalent lanthanide ions[17–19] and of divalent transition metal ions.[1–3,20–26] By taking advantage of the variation of the coordination number through a proper choice of the metal ion, one can obtain complexes with different metal-to-ligand ratios and molecular geometries, and thus, modifications in the mesophase behavior are expected. However, in order to study the influence of the metal ion on the thermal behavior of metallomesogens, it is necessary to have ligand systems that are able to form complexes with many different types of metal ions. Good examples are provided by the metal alkanoates, for which covalent or ionic bonding between the metal and the carboxylate groups is observed, depending on the choice of the metal.[3,16] Also, varying the oxidation state of the metal yields ML, ML_2 and M_2L_4, and ML_3 complexes having metal-to-ligand ratios of 1:1, 1:2, and 1:3, respectively. Another versatile system is provided by metal β-diketonates, for which complexes with metal-to-ligand ratios varying between 1:1 and 1:4 have been prepared.[27–35]

It is known that 1,10-phenanthrolines are able to form complexes with a variety of metal ions.[36] However, there are only a few examples of metallomesogens with 1,10-phenanthroline derivatives as ligands,[37–40] and the number of mesomorphic metal-free 1,10-phenanthrolines is also limited.[38,41] The development of liquid-crystalline 1,10-phenanthrolines has been hampered by synthetic difficulties, mainly involving solubility problems and the formation of unwanted side products. We explored a published approach for functionalizing 1,10-phenanthrolines that is based on 2-arylimidazo[4,5-*f*]-1,10-phenanthroline heterocycles.[38,39,42] 2-Arylimidazo[4,5-*f*]-1,10-phenanthroline can easily be prepared in one step, and the possibility of varying the substitution pattern directly at the benzaldehyde-precursor stage provides easy access to a rich variety of building blocks. These ligands have been used in the past for formation of complexes with ruthenium(II)[43] and as a coligand in luminescent lanthanide(III) complexes.[44]

Here we discuss the influence of the metal ion and the geometry of the complex, the substitution pattern, and the length of the alkoxy chain on the mesomorphic properties of imidazo[4,5-*f*]-1,10-phenanthroline-based derivatives. The structure and thermal behavior of these compounds differed from those of the related imidazo[4,5-*f*]-1,10-phenanthrolines bearing 4-cyanobiphenyl groups connected via a long alkyl spacer, on which we have reported previously.[38] The compounds presented in this paper had a metal-to-ligand ratio of 1:1 or 1:2, depending on the metal ion: a 1:1 square-planar platinum(II) complex, 1:1 octahedral rhenium(I) complexes, and 1:2 trivalent lanthanide complexes were studied. A 1:3 uranyl complex of the type $[ML_3]^{2+}$ that was described in an earlier communication[39] has also been included here, in order to facilitate the discussion of the relationship between molecular structure and mesomorphism. Self-assembled monolayers of a europium(III) complex were studied by scanning tunneling microscopy (STM), and the photophysical properties of the rhenium(I) complexes and lanthanide(III) complexes were investigated.

Experimental Section

General Procedures. Nuclear magnetic resonance (NMR) spectra were recorded on a Bruker Avance 300 spectrometer (operating at 300 MHz for ^{1}H) or a Bruker AMX-400 spectrometer (operating at 400 MHz for ^{1}H). Elemental analyses were obtained using a CE Instruments EA-1110 elemental analyzer. Optical textures of the mesophases were observed with an Olympus BX60 polarizing microscope equipped with a Linkam THMS600 hot stage and a Linkam TMS93 programmable temperature controller. Differential scanning calorimetry (DSC) traces were recorded with a Mettler-Toledo DSC822e module. Electrospray ionization (ESI) spectra were recorded on a Thermo Finnigan LCQ Advantage mass spectrometer.

All STM experiments were performed at 20–22 °C using a PicoSPM apparatus (Molecular Imaging). STM tips (80:20 Pt/Ir, 0.2 mm diameter) were prepared by mechanical cutting. Prior to imaging, the compound was dissolved in 1-phenyloctane or octanoic acid at a concentration of 1 mg g^{-1}. A drop of the solution was

(17) Binnemans, K.; Van Deun, R.; Bruce, D. W.; Galyametdinov, Y. G. *Chem. Phys. Lett.* **1999**, *300*, 509–514.
(18) Binnemans, K.; Sleven, J.; De Feyter, S.; De Schryver, F. C.; Donnio, B.; Guillon, D. *Chem. Mater.* **2003**, *15*, 3930–3938.
(19) Terazzi, E.; Torelli, S.; Bernardinelli, G.; Rivera, J. P.; Benech, J. M.; Bourgogne, C.; Donnio, B.; Guillon, D.; Imbert, D.; Bünzli, J. C. G.; Pinto, A.; Jeannerat, D.; Piguet, C. *J. Am. Chem. Soc.* **2005**, *127*, 888–903.
(20) Bruce, D. W. Metal-Containing Liquid Crystals. In *Inorganic Materials*, 2nd ed.; Bruce, D. W., O'Hare, D., Eds.; Wiley: Chichester, U.K., 1996; pp 429–522.
(21) Donnio, B.; Bruce, D. W. *J. Chem. Soc., Dalton Trans.* **1997**, 2745–2755.
(22) Donnio, B.; Bruce, D. W. *Struct. Bonding* **1999**, *95*, 193–247.
(23) Giroud-Godquin, A. M.; Maitlis, P. M. *Angew. Chem., Int. Ed.* **1991**, *30*, 375–402.
(24) Hudson, S. A.; Maitlis, P. M. *Chem. Rev.* **1993**, *93*, 861–885.
(25) Morale, F.; Date, R. W.; Guillon, D.; Bruce, D. W.; Finn, R. L.; Wilson, C.; Blake, A. L.; Schroder, M. W.; Donnio, B. *Chem.—Eur. J.* **2003**, *9*, 2484–2501.
(26) Sleven, J.; Cardinaels, T.; Görller-Walrand, C.; Binnemans, K. *ARKIVOC* **2003**, *2003* (iv), 68–82.
(27) Serrano, J. L.; Sierra, T. *Chem.—Eur. J.* **2000**, *6*, 759–766.
(28) Barbera, J.; Elduque, A.; Gimenez, R.; Lahoz, F. J.; Lopez, J. A.; Oro, L. A.; Serrano, J. L.; Villacampa, B.; Villalba, J. *Inorg. Chem.* **1999**, *38*, 3085–3092.
(29) Trzaska, S. T.; Zheng, H. X.; Swager, T. M. *Chem. Mater.* **1999**, *11*, 130–134.
(30) Trzaska, S. T.; Swager, T. M. *Chem. Mater.* **1998**, *10*, 438–443.
(31) Zheng, H. X.; Lai, C. K.; Swager, T. M. *Chem. Mater.* **1995**, *7*, 2067–2077.
(32) Atencio, R.; Barbera, J.; Cativiela, C.; Lahoz, F. J.; Serrano, J. L.; Zurbano, M. M. *J. Am. Chem. Soc.* **1994**, *116*, 11558–11559.
(33) Zheng, H. X.; Swager, T. M. *J. Am. Chem. Soc.* **1994**, *116*, 761–762.
(34) Ohta, K.; Muroki, H.; Takagi, A.; Hatada, K. I.; Ema, H.; Yamamoto, I.; Matsuzaki, K. *Mol. Cryst. Liq. Cryst.* **1986**, *140*, 131–152.
(35) Ohta, K.; Ishii, A.; Muroki, H.; Yamamoto, I.; Matsuzaki, K. *Mol. Cryst. Liq. Cryst.* **1985**, *116*, 299–307.
(36) Sammes, P. G.; Yahioglu, G. *Chem. Soc. Rev.* **1994**, *23*, 327–334.
(37) Date, R. W.; Iglesias, E. F.; Rowe, K. E.; Elliott, J. M.; Bruce, D. W. *Dalton Trans.* **2003**, 1914–1931.
(38) Cardinaels, T.; Driesen, K.; Parac-Vogt, T. N.; Heinrich, B.; Bourgogne, C.; Guillon, D.; Donnio, B.; Binnemans, K. *Chem. Mater.* **2005**, *17*, 6589–6598.
(39) Cardinaels, T.; Ramaekers, J.; Guillon, D.; Donnio, B.; Binnemans, K. *J. Am. Chem. Soc.* **2005**, *127*, 17602–17603.
(40) Ziessel, R.; Pickaert, G.; Camerel, F.; Donnio, B.; Guillon, D.; Cesario, M.; Prange, T. *J. Am. Chem. Soc.* **2004**, *126*, 12403–12413.
(41) Bousquet, S. J. P.; Bruce, D. W. *J. Mater. Chem.* **2001**, *11*, 1769–1771.
(42) Bian, Z. Q.; Wang, K. Z.; Jin, L. P.; Gao, L. H. *Synth. Commun.* **2003**, *33*, 3477–3482.
(43) Hiort, C.; Lincoln, P.; Norden, B. *J. Am. Chem. Soc.* **1993**, *115*, 3448–3454.
(44) Lenaerts, P.; Storms, A.; Mullens, J.; D'Haen, J.; Görller-Walrand, C.; Binnemans, K.; Driesen, K. *Chem. Mater.* **2005**, *17*, 5194–5201.

applied onto a freshly cleaved surface of highly oriented pyrolytic graphite (HOPG, grade ZYB, Advanced Ceramics Inc., Cleveland, OH). The STM tip was immersed in the solution, and images were recorded at the liquid–solid interface. The STM images were acquired in variable-height mode. The measured heights were converted into a gray scale. To check for reproducibility and avoid artifacts, the experiments were repeated over several sessions using several tips. To facilitate analysis, recording of a monolayer image was followed by imaging of the underlying graphite substrate using the same experimental conditions, except for a lower bias voltage. The images were corrected for drift via Scanning Probe Image Processor (SPIP) software (Image Metrology ApS), using the recorded graphite images for calibration purposes, allowing a more accurate unit-cell determination. The imaging parameters (bias voltage and tunneling-current setpoint) are indicated in the figure captions.

X-ray diffraction (XRD) patterns were obtained using two different experimental setups, and in all cases, the powdered sample was contained in Lindemann capillaries having a diameter of 1 mm and a wall thickness of 10 μm. A linear monochromatic Cu Kα_1 beam ($\lambda = 1.5405$ Å) obtained with a sealed-tube generator (900 W, Inel) and a bent quartz monochromator (Inel) were used. One set of diffraction patterns was registered with an Inel CPS 120 curved counter, for which the sample temperature was controlled within $\pm$0.05 °C from 20 to 200 °C; periodicities up to 60 Å could be measured. The other set of diffraction patterns was registered on an image plate. Periodicities up to 90 Å could be measured, and the sample temperature was controlled within $\pm$0.3 °C from 20 to 350 °C.

Crystal Data for Compounds [Eu(tta)$_3$L$_{XIII}$], [ReBr(CO)$_3$ L$_{XIII}$], and L$_I$. Yellow single crystals of [Eu(tta)$_3$L$_{XIII}$]·MeOH (where tta is 2-thenoyltrifluoroacetonate), [ReBr(CO)$_3$L$_{XIII}$]·DMF, and L$_I$·EtOH were obtained by slow evaporation of solutions of the compounds in methanol (MeOH), dimethylformamide (DMF), and ethanol (EtOH), respectively, in a refrigerator at 4 °C. X-ray intensity data were collected on a SMART 6000 diffractometer equipped with a CCD detector using Cu Kα radiation ($\lambda = 1.54178$ Å). The images were interpreted and integrated with the program SAINT from Bruker.[45]

[Eu(tta)$_3$L$_{XIII}$]·MeOH: $C_{46}H_{36}EuF_9N_4O_9S_3$, $M = 1205.24$ g mol^{-1}, triclinic, $P\bar{1}$ (No. 2), $a = 10.8917(8)$ Å, $b = 15.6770(11)$ Å, $c = 15.9877(8)$ Å, $\alpha = 117.819(3)°$, $\beta = 97.656(4)°$, $\gamma = 93.066(5)°$, $V = 2371.9(3)$ Å^3, $T = 100(2)$ K, $Z = 2$, $\rho_{calc} = 1.688$ g cm^{-3}, μ(Cu Kα) = 11.548 mm^{-1}, $F(000) = 1205$, crystal size $0.4 \times 0.25 \times 0.2$ mm, 8621 independent reflections ($R_{int} = 0.0951$). Final $R = 0.0581$ for 7168 reflections with $I > 2\sigma(I)$ and wR2 = 0.1454 for all data.

[ReBr(CO)$_3$L$_{XIII}$]·DMF: $C_{25}H_{19}BrN_5O_4Re$, $M = 719.56$ g mol^{-1}, triclinic, $P\bar{1}$ (No. 2), $a = 8.890(6)$ Å, $b = 10.729(7)$ Å, $c = 13.263(8)$ Å, $\alpha = 81.23(4)°$, $\beta = 71.34(4)°$, $\gamma = 80.52(4)°$, $V = 1175.4(13)$ Å^3, $T = 100(2)$ K, $Z = 2$, $\rho_{calc} = 2.033$ g cm^{-3}, μ(Cu Kα) = 12.479 mm^{-1}, $F(000) = 692$, crystal size $0.4 \times 0.2 \times 0.2$ mm, 3796 independent reflections ($R_{int} = 0.0734$). Final $R = 0.0556$ for 3236 reflections with $I > 2\sigma(I)$ and wR2 = 0.1803 for all data.

L$_I$·EtOH: $C_{37}H_{50}N_4O_2$, $M = 582.81$ g mol^{-1}, triclinic, $P\bar{1}$ (No. 2), $a = 9.9760(13)$ Å, $b = 11.2810(13)$ Å, $c = 15.387(2)$ Å, $\alpha = 70.760(8)°$, $\beta = 81.138(8)°$, $\gamma = 84.700(9)°$, $V = 1613.8(4)$ Å^3, $T = 100(2)$ K, $Z = 2$, $\rho_{calc} = 1.199$ g cm^{-3}, μ(Cu Kα) = 0.577 mm^{-1}, $F(000) = 632$, crystal size $0.4 \times 0.25 \times 0.15$ mm, 5869 independent reflections ($R_{int} = 0.0741$). Final $R = 0.0682$ for 3358 reflections with $I > 2\sigma(I)$ and wR2 = 0.1960 for all data.

All three structures were solved by direct methods and refined by full-matrix least-squares analysis on F^2 using the SHELXTL program package.[46] Non-hydrogen atoms were anisotropically refined, and the hydrogen atoms in the riding mode with isotropic temperature factors were fixed at $1.2 \times U_{eq}$ of the parent atoms [$1.5 \times U_{eq}$ for methyl groups]. Crystallographic information files are provided in the Supporting Information.

Synthetic Procedures. All chemicals were purchased from Acros Organics.

(1) Synthesis of Ligands L$_I$−L$_{XI}$. The appropriate alkoxybenzaldehyde (1 equiv) was added to a warm solution of 1,10-phenanthroline-5,6-dione[43] (**2**) (1 equiv) and ammonium acetate (8.5 equiv) in glacial acetic acid, and then the mixture was heated to 85 °C for 5 h. After the reaction mixture was cooled to room temperature, it was poured into 100 mL of water and neutralized to pH 7 with an aqueous ammonia solution. The precipitate was filtered off, washed with distilled water, and dried. The crude product was purified on a silica column using 50:50:10 $CHCl_3$/hexane/MeOH as the eluent. Because the compound held solvents firmly, it was dried in a vacuum oven at 50 °C. Analytical data for ligands L$_I$−L$_{XI}$ are available in the Supporting Information.

(2) Synthesis of Ligand L$_{XII}$. Under a nitrogen atmosphere, sodium hydride (0.75 mmol, 0.030 g of a 60% dispersion in mineral oil) was added to a solution of ligand L$_{VI}$ (0.36 mmol, 0.28 g) in dry DMF (10 mL), and the mixture was heated to 100 °C under a nitrogen atmosphere. Ethylbromide (0.46 mmol, 0.050 g) was then added dropwise, and the mixture was heated to reflux for 12 h under a nitrogen atmosphere. NaBr that formed upon cooling was filtered off, and the solvent was removed under reduced pressure. The crude product was purified on a silica column using 50:50:10 $CHCl_3$/hexane/MeOH as the eluent. Analytical data for ligand L$_{XII}$ are available in the Supporting Information.

(3) Synthesis of the Platinum(II) Complex [PtCl$_2$L$_{XI}$]. A solution of [PtCl$_2$(NCPh)$_2$] (0.140 mmol, 0.066 g) in chloroform was added to a solution of ligand L$_{XI}$ (0.107 mmol, 0.100 g) in chloroform, and the mixture was refluxed for 5 h. The solvent was then removed under reduced pressure, and diethyl ether was added. Excess [PtCl$_2$(NCPh)$_2$] was removed by filtration, and ethanol was added until precipitation occurred. The orange precipitate was filtered off and dried in a vacuum oven at 50 °C. Analytical data for the platinum(II) complex are available in the Supporting Information.

(4) Synthesis of the Rhenium(I) Complexes. Rhenium(I) pentacarbonyl bromide (1 equiv) was added to a solution of the appropriate ligand (1 equiv) in toluene, and the mixture was refluxed for 3 h. The solvent was then removed under reduced pressure, and the crude product was purified on a silica column using 50:50 $CHCl_3$/hexane as the eluent. The complex was dissolved in a minimum amount of $CHCl_3$ and precipitated in hexane or ethanol. The yellow precipitate was filtered off and dried in a vacuum oven at 50 °C. Analytical data for the rhenium(I) complexes are available in the Supporting Information.

(5) Synthesis of the Lanthanide(III) Complexes. A solution of $LnCl_3 \cdot xH_2O$ (1 equiv) in ethanol was added to a solution of the appropriate ligand (2 equiv) in hot ethanol, and the solution was stirred for 30 min at 65 °C. The yellow/orange precipitate that formed was filtered off, washed with ethanol, and dried in a vacuum oven at 50 °C. Analytical data for the lanthanide(III) complexes are available in the Supporting Information.

(6) Synthesis of the Uranyl Complex. A solution of $UO_2(CF_3SO_3)_2$[47] (0.036 mmol, 0.020 g) in ethanol was added to a

(45) *SAINT*, version 5/6.0; Bruker Analytical X-ray Systems Inc.: Madison, WI, 1997.

(46) *SHELXTL-PC*, version 5.1; Bruker Analytical X-ray Systems Inc.: Madison, WI, 1997.

(47) Berthet, J. C.; Lance, M.; Nierlich, M.; Ephritikhine, M. *Eur. J. Inorg. Chem.* **2000**, 1969–1973.

Scheme 1. Synthesis of the Imidazo[4,5-*f*]-1,10-phenanthroline Ligands

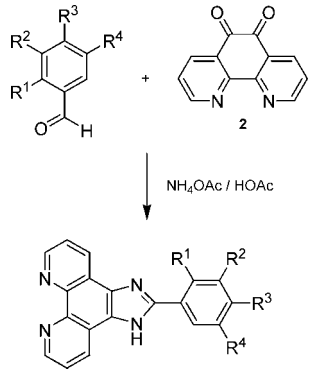

warm solution of ligand L_{XI} (0.107 mmol, 0.100 g) in ethanol, and the mixture was stirred for 30 min at 65 °C. The orange precipitate that formed was filtered off, washed with ethanol, and dried in a vacuum oven at 50 °C. Analytical data for the uranyl complex are available in the Supporting Information.

(7) Synthesis of the Europium(III) Complex [Eu(tta)$_3$L$_{III}$]. $[Eu(tta)_3(H_2O)_2]$[48] (1 equiv) was dissolved in ethanol and added slowly to a solution of ligand L_{III} (1 equiv) in hot ethanol, and the mixture was stirred for 30 min at 65 °C. After the mixture was cooled to room temperature, a yellow precipitate formed and was filtered off, washed with ethanol, and dried in a vacuum oven at 50 °C. Analytical data for the europium(III) complex are available in the Supporting Information.

Results and Discussion

Synthesis and Characterization of the Ligands. Each 2-arylimidazo[4,5-*f*]-1,10-phenanthroline was prepared by a condensation reaction between 1,10-phenanthroline-5,6-dione **2** and the appropriate polyalkoxylated benzaldehyde in the presence of ammonium acetate and glacial acetic acid (Scheme 1). The synthetic route was similar to the method reported by Steck and Day for the preparation of 2-substituted phenanthrimidazoles.[49] 1,10-Phenanthroline (**1**) was oxidized to **2** according to a method described by Hiort et al.[43] Structure variations included the choice of different chain substitution patterns for the benzaldehyde as well as variation of the alkoxy chain length. 4-Hydroxybenzaldehyde (**3**), 3,4-dihydroxybenzaldehyde (**4**), 3,5-dihydroxybenzaldehyde (**5**), 2,3,4-trihydroxybenzaldehyde (**6**), 2,4,5-trihydroxybenzaldehyde (**7**), and 3,4,5-trihydroxybenzaldehyde (**8**) were used as starting products. They were prepared as their tetradecyloxypolyether (L_V, L_{VIII}, L_{IX}, L_X, L_{XI}) or hexadecyloxyether (L_I) homologues. The 3,4-dialkoxybenzaldehyde series was prepared with the alkoxy chains OC_2H_5, OC_6H_{13}, $OC_{10}H_{21}$, $OC_{14}H_{29}$, $OC_{16}H_{33}$, and $OC_{18}H_{37}$ (L_{II}, L_{III}, L_{IV}, L_V, L_{VI}, and L_{VII}, respectively). We also investigated the influence of alkylation of the N atom of the five-membered imidazole ring. An overview of the different ligands is given in Figure 1. All of the imidazo[4,5-*f*]-1,10-phenanthrolines were characterized by CHN analysis, ^{1}H and ^{13}C NMR spectroscopy, and mass spectrometry (see the Supporting Information).

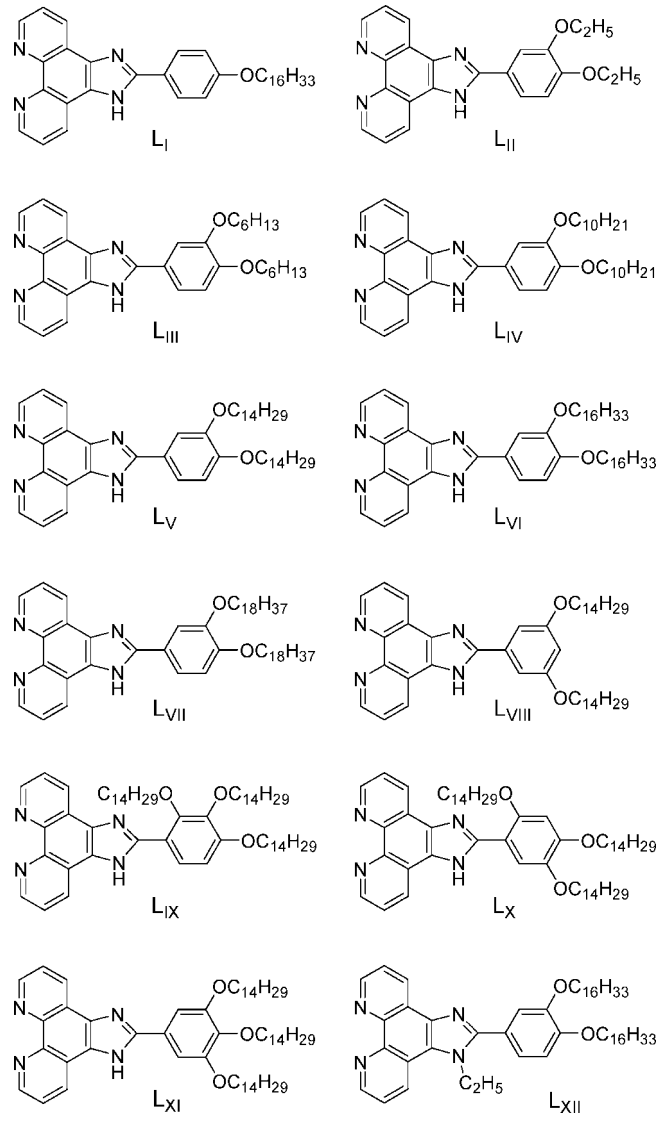

Figure 1. Overview of the imidazo[4,5-*f*]-1,10-phenanthroline ligands.

Recently, we reported on the synthesis of liquid-crystalline imidazo[4,5-*f*]-1,10-phenanthrolines containing mesogenic 4-cyanobiphenyl groups.[38] This synthesis was successfully applied for imidazo[4,5-*f*]-1,10-phenanthrolines containing only aliphatic chains. However, the solubilities of these two classes of ligands are very different. The imidazo[4,5-*f*]-1,10-phenanthrolines containing mesogenic 4-cyanobiphenyl groups are soluble only in dichloromethane, chloroform, tetrahydrofuran, and hot toluene. Therefore, metal complexes involving the 4-cyanobiphenyl-substituted ligands were prepared for only those cases in which the corresponding metal salt precursors were soluble in solvents that can dissolve the ligand: complexes of lanthanide(III) ions (with tta as coligand) and rhenium(I). The corresponding metal precursors $[Ln(tta)_3(H_2O)_2]$ and $[ReBr(CO)_5]$ are soluble in chloroform and toluene, respectively, which are solvents that also dissolve the ligands. Unfortunately, many metal salts, such as *cis*-$[RuCl_2(bipy)_2]$, $LnCl_3 \cdot xH_2O$, and $UO_2(CF_3SO_3)_2$, are soluble only in water, methanol, or ethanol, rendering the preparation of the corresponding coordination complexes rather difficult. The imidazo[4,5-*f*]-1,10-phenanthrolines containing only aliphatic chains are soluble in diethyl ether,

(48) Melby, L. R.; Rose, N. J.; Abramson, E.; Caris, J. C. *J. Am. Chem. Soc.* **1964**, *86*, 5117–5125.
(49) Steck, E. A.; Day, A. R. *J. Am. Chem. Soc.* **1943**, *65*, 452–456.

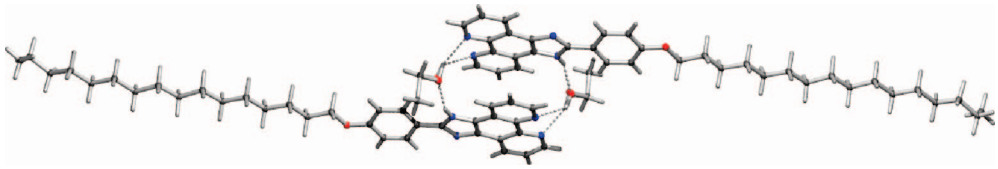

Figure 2. Molecular structure of dimers of ligand L_I. The bridging by ethanol molecules in dimers of the ligand is shown.

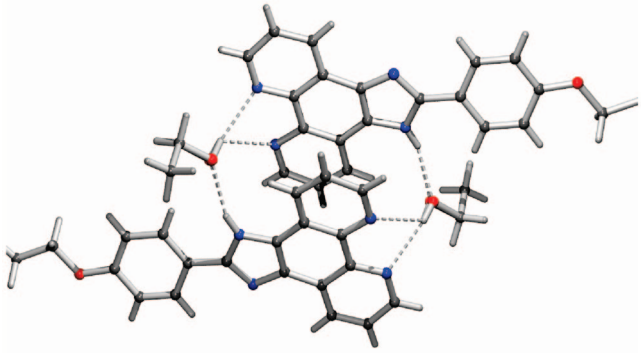

Figure 3. Molecular structure of dimers of ligand L_I. The ligands are bridged to form dimers via hydrogen bonding by ethanol molecules. This view focuses on the hydrogen-bonding region of the dimers; the ligand alkyl chains extend to the left and right beyond the edges of the figure.

hexane, and warm ethanol in addition to dichloromethane, chloroform, tetrahydrofuran, and toluene, enabling complexes of the lanthanide(III) and uranyl ions to be prepared without experiencing solubility problems. We tried to obtain $Ln(tta)_3$ complexes with ligand L_{XI}, but all of the trials were unsuccessful because of the high solubility of this type of lanthanide(III) complex; the complexes could not be selectively precipitated, and as a result, the complexes obtained by precipitation upon addition of ethanol were always contaminated by traces of free ligand. The $Eu(tta)_3$ complex of ligand L_{III} could be obtained in good purity, but this europium(III) complex is not mesomorphic. For the ligands with short alkyl chains, the lanthanide(III) complexes had lower solubilities than the ligands, which meant that these complexes could be selectively precipitated.

It should be mentioned that all the ligands bound 0.5 equiv of water (determined by CHN analysis). The bonded water molecule could not be removed, even after a long drying period in a vacuum oven at a temperature lower than the melting point of the compounds. On the basis of the molecular structure of L_I (Figures 2 and 3), which was determined by single-crystal X-ray diffraction, it is very likely that all of the ligands form dimers in which a water molecule connects two ligands via strong hydrogen bonds. A strong intermolecular N−H···O hydrogen bond appears between the hydrogen atom attached to the imidazo nitrogen of one ligand and an ethanol solvent molecule (H···O distance: 2.01 Å). This ethanol molecule is also connected by hydrogen bonds to the nitrogens of the phenanthroline part of a second L_I ligand (H···N distance: 2.26 Å), and the resulting dimer is arranged with the alkyl chains pointing in opposite directions. The asymmetric unit contains one crystallographically independent molecule.

The ^1H and ^{13}C NMR spectra of L_{XII} (in which one of the N atoms of the imidazole ring is alkylated with an ethyl group) were compared with the spectra of all of the other ligands (in which there is no alkylation of the N atoms of the imidazole ring). For L_{XII}, all of the heteroaromatic carbons (six tertiary and seven quaternary carbon atoms of imidazo[4,5-*f*]-1,10-phenanthroline) could be assigned via two-dimensional (2D) $^1H-^{13}C$ correlation spectroscopy (HMQC and HMBC). For the other ligands, an intermolecular exchange reaction involving the N−H hydrogen atom occurs between the two N atoms of the imidazole ring (*prototropic tautomerism*).[50] The rate of this exchange reaction depends on many factors, such as concentration, solvent, and temperature. In the case of a fast exchange reaction, three resonances assigned to tertiary carbon atoms and four resonances assigned to quaternary carbon atoms should have been observed in the ^{13}C NMR spectrum, and their chemical shifts should have been the averages of the corresponding values for ligand L_{XII}. For a very slow exchange reaction, the chemical shift values were expected to be similar to those of the ligand L_{XII}. For an intermediate exchange rate (the most frequently observed situation), broadened resonances for the tertiary and quaternary carbon atoms were observed at an average value, but usually the two resonances of quaternary carbon atoms of the imidazole ring were broadened beyond detection. The resonance of the quaternary carbon atom between the two N atoms (i.e., in the 2-position of the imidazole ring) was not affected by the exchange process and produced a sharp signal at 152–154 ppm. For all of the ligands, the carbons of the substituted aryl group attached to the imidazo[4,5-*f*]-1,10-phenanthroline gave sharp signals.

Synthesis and Characterization of the Metal Complexes. The platinum(II) complex was synthesized by a ligand-exchange reaction between ligand L_{XI} and $[PtCl_2(NCPh)_2]$ (1:1.3 molar ratio) in chloroform. The rhenium(I) complexes were synthesized by reaction between the corresponding ligand and $[ReBr(CO)_5]$ (1:1 molar ratio) in toluene. The lanthanide(III) complexes were prepared by reaction between the corresponding ligand and $LnCl_3 \cdot xH_2O$ (2:1 molar ratio; Ln = La, Pr, Nd, Sm, Eu, Gd, Tb, Dy, Ho) in ethanol. The $[Eu(tta)_3L_{III}]$ complex was synthesized by reaction between ligand L_{III} and $[Eu(tta)_3(H_2O)_2]$ (1:1 molar ratio) in ethanol. The uranyl complex was prepared by reaction between ligand L_{XI} and uranyl triflate (3:1 molar ratio) in ethanol.[39] All of the metal complexes were characterized by CHN analysis and mass spectrometry (see the Supporting Information). The uranyl complex was additionally characterized by IR spectroscopy and ^1H and ^{13}C NMR spectroscopy (see the Supporting Information). Except for the uranyl complex, all of the metal complexes contained water (the amounts of which were determined by CHN analysis), for the same reason as that given for the ligands.

(50) Katritzky, A. R.; Karelson, M.; Harris, P. A. *Heterocycles* **1991**, *32*, 329–369.

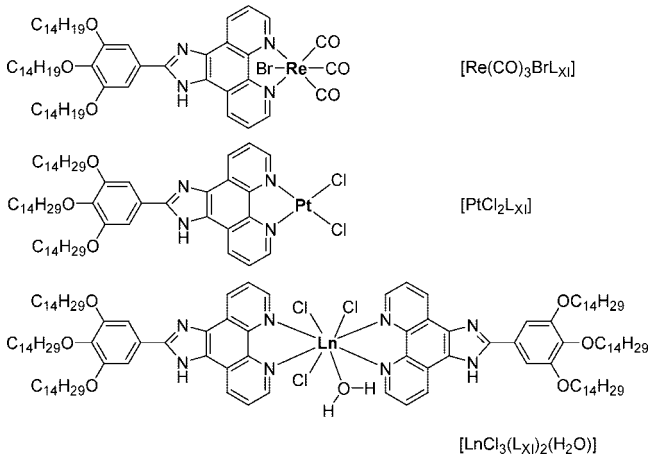

Figure 4. Overview of the different types of metal complexes, with ligand L_{XI} as the complexing ligand.

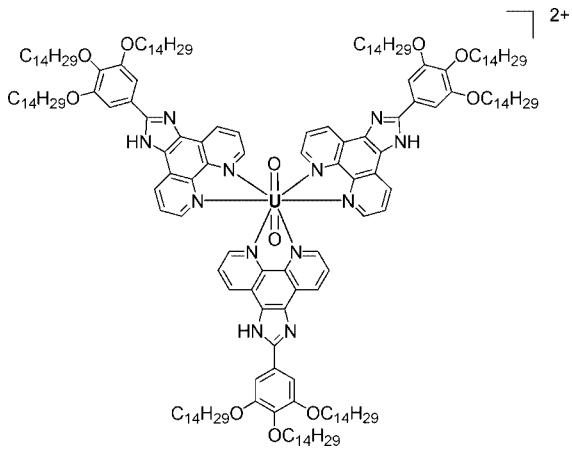

Figure 5. Structure of the uranyl complex. The two noncoordinating triflate counterions have been omitted.

Due to its unconventional propeller-like structure, it was possible to obtain the uranyl complex free of bonded water molecules. An overview of the different types of metal complexes (with ligand L_{XI} as the complexing ligand) is given in Figure 4. Figure 5 shows the structure of the uranyl complex.

Single crystals of the rhenium(I) complex $[ReBr(CO)_3L_{XIII}]$ and the europium(III) complex $[Eu(tta)_3L_{XIII}]$ (where L_{XIII} is phenylimidazo[4,5-*f*]-1,10-phenanthroline) were obtained and examined by XRD. In the molecular structure of the rhenium(I) complex $[ReBr(CO)_3L_{XIII}]$, three carbonyl ligands, one bromide ion, and one L_{XIII} ligand are coordinated to the rhenium(I) ion (Figure 6). The coordination number of the rhenium(I) ion is 6, and the coordination polyhedron can be described as a slightly distorted octahedron. Strong intermolecular N−H···O hydrogen bonds appear between the hydrogen atom of the imidazo nitrogen and the oxygen of a DMF solvent molecule (H···O distance: 1.93 Å). In addition, pairs of complexes show weak, antiparallel $\pi-\pi$-stacking interactions within a distance of about 3.5 Å (Figure 7).

The molecular structure of $[Eu(tta)_3L_{XIII}]$ shows very clearly that three bidentate tta ligands and one L_{XIII} ligand are coordinated to the europium(III) ion (Figure 8). The coordination number of the europium(III) ion is 8, and the coordination polyhedron can be described as a distorted

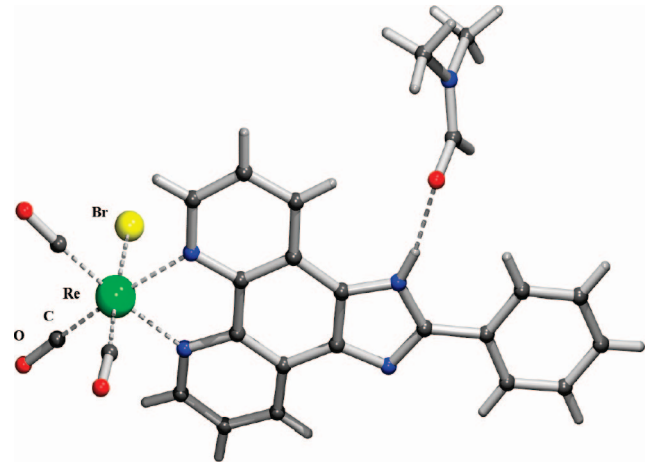

Figure 6. Molecular structure of the rhenium(I) complex $[ReBr(CO)_3L_{XIII}]\cdot DMF$.

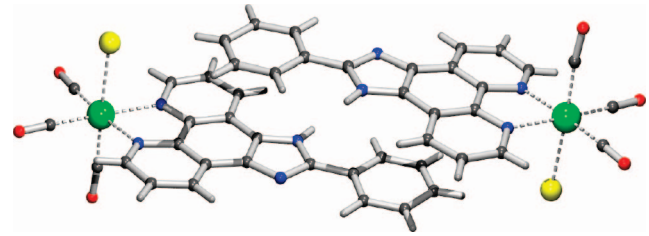

Figure 7. Antiparallel $\pi-\pi$-stacking of rhenium(I) complexes $[ReBr(CO)_3L_{XIII}]$.

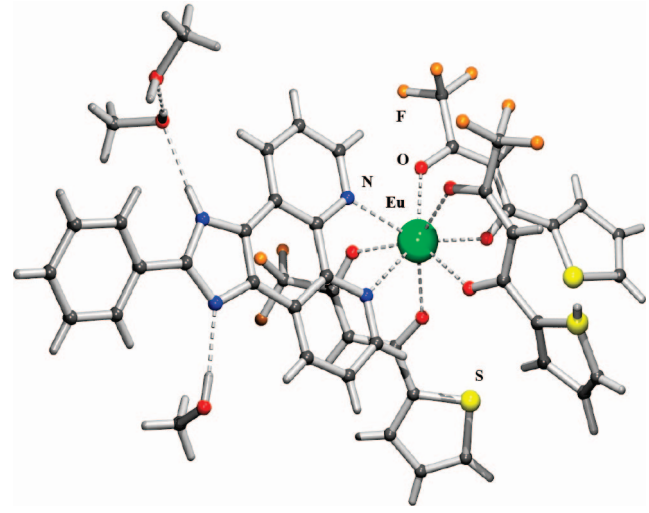

Figure 8. Molecular structure of the europium(III) complex $[Eu(tta)_3L_{XIII}]\cdot MeOH$. The hydrogen bonding by solvent molecules is shown.

square antiprism. Strong intermolecular N−H···O and N···H−O hydrogen bonds appear between the imidazo nitrogens and methanol solvent molecules (average H···O distance: 1.94 Å). These methanol molecules are also bridged by hydrogen bonds to those of a second $[Eu(tta)_3L_{XIII}]$ complex, and the resulting dimers are arranged with the L_{XIII} ligands pointing in opposite directions (Figure 9). The packing of $[Eu(tta)_3L_{XIII}]$ in the crystal structure is shown in Figure 10.

All attempts to grow single crystals for the other complexes failed. Actually, very few examples of crystal structures of imidazo[4,5-*f*]-1,10-phenanthrolines have been

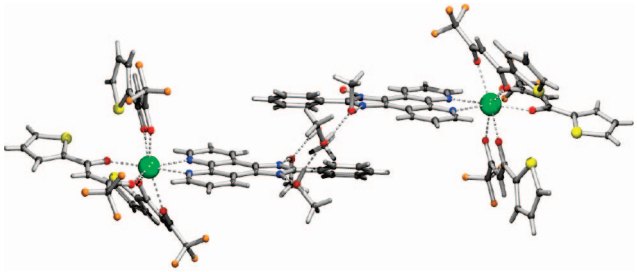

Figure 9. Molecular structure of dimers of the europium(III) complex $[Eu(tta)_3L_{XIII}]\cdot MeOH$. The bridging by hydrogen-bonded solvent molecules and the arrangement in the dimers are shown.

published.[51,52] The platinum(II) complex is very likely to have a square-planar geometry, because all of the reported crystal structures of platinum(II) complexes with 1,10-phenanthroline show a square-planar coordination sphere for platinum(II).[53,54] As for the lanthanide(III) complexes, the reported structure with the closest similarity is that of $[LaCl_3(phen)_2(H_2O)]\cdot MeOH$.[55] In this compound, the lanthanum(III) ion is coordinated to three chloride ions, one water molecule, and two 1,10-phenanthroline ligands. The two 1,10-phenanthroline rings are positioned approximately perpendicular to each other. In the lanthanide(III) chloride complexes presented in this work, there is very likely one molecule of water directly coordinated to the lanthanide(III) ion. If there is no water molecule present in the first coordination sphere, the coordination number of the lanthanide(III) ion would be only 7, which is rather low (the coordination number is usually 8 or 9). Also, in the crystal structure of $[LaCl_3(phen)_2(H_2O)]\cdot MeOH$, one water molecule is present in the first coordination sphere. For the uranyl complex, it is reasonable to assume that the first coordination sphere is comparable to that observed for the $[UO_2(phen)_3](OTf)_2$ complex, with an equal population of right- and left-handed helices.[56,57] The coordination polyhedron can be described as a bi-end-capped trigonal antiprism.

Scanning Tunneling Microscopy. Alkylated molecules are known to show a good affinity for HOPG. Upon their adsorption, STM often provides structural information with submolecular resolution. As an example, we investigated self-assembly of $EuCl_3(L_{XI})_2(H_2O)$ at the solid–liquid interface. Figure 11 shows STM images of a self-assembled monolayer of $EuCl_3(L_{XI})_2(H_2O)$ formed at the graphite−1-phenyloctane interface. A regular pattern of bright and dark areas was observed. In these current images, bright (dark) areas correlated with large (small) tunneling currents. Generally, aromatic moieties are characterized by a relatively large tunneling current, while alkyl chains are typically less transmissive for tunneling electrons. Thus, in these images the bright features were attributed to the aromatic moieties of the ligands and the central ion, while the darker areas corresponded to the aliphatic chains. The high contrast of the central core of this molecule resulted from both the high electron density and the specific morphology, since the L_{XI} ligands in the complex were not expected to be fully coplanar with the surface. The complex formed clusters and curved lamellae. The surface layer lacked long-range order. The size of these clusters ranged from 3.3 to 5.5 nm, suggesting that they did not correspond to single molecules but were composed of 2−5 molecules. In some areas alkyl chains could be visualized.

In contrast, when the solvent was changed to octanoic acid, a regular well-ordered pattern appeared almost immediately (Figure 12). Rhombus-shaped bright features were visible: their long and short axes measured 4 and 2 nm, respectively. After calibration versus the graphite lattice, the unit-cell parameters of this 2D crystal were found to have the following values: $a = 4.8 \pm 0.2$ nm, $b = 5.0 \pm 0.2$ nm, and $\theta = 55 \pm 3°$. From the high-resolution image, the aliphatic chains were resolved with near atomic resolution. There were 16 alkyl chains per bright rhombus, four of which ran along the *a* axis of the unit cell. This clearly indicated that the bright features were not single molecules. In view of the core size of the complex (nearly 2.5 nm in length and 1 nm in width) and the number of alkyl chains, the bright features were attributed to dimers of the complex. Four of the alkyl chains were considered to be coadsorbed solvent molecules. Coadsorption is believed to have been promoted by hydrogen-bonding interactions between the carboxylic acid groups of the solvent molecules and the nitrogen atoms of the aromatic ligands. These observations are in line with the lack of ordering observed at the graphite−1-phenyloctane interface.

Thermal Behavior of the Ligands. The thermal behavior of the ligands was studied using polarizing optical microscopy (POM), DSC, and XRD. The results of these investigations are given in Table 1.

Essentially all of the ligands were devoid of mesomorphism. In the solid state, the molecules were arranged into dimers, which were stabilized by water molecules via hydrogen bonding (as described above). Such supramolecular dimers can be considered as polycatenar systems in which alkoxy chains are attached at both sides of the rodlike core built up by two phenylimidazo[4,5-*f*]-1,10-phenanthroline units. Polycatenar systems have been well investigated in the past, and it is known that in order to induce mesomorphism, the rodlike core should contain at least four aromatic rings.[58–60] In the present study, the aspect ratio of the ligands was rather small, primarily because of the bulky imidazophenanthroline core; this was a likely factor limiting the tendency to form liquid-crystalline phases.

(51) Chao, H.; Yuan, Y. X.; Ji, L. N. *Transition Met. Chem.* **2004**, *29*, 774–779.
(52) Xu, H.; Zheng, K. C.; Chen, Y.; Li, Y. Z.; Lin, L. J.; Li, H.; Zhang, P. X.; Ji, L. N. *Dalton Trans.* **2003**, 2260–2268.
(53) Gaballa, A.; Wagner, C.; Schmidt, H.; Steinborn, D. *Z. Anorg. Allg. Chem.* **2003**, *629*, 703–710.
(54) Fanizzi, F. P.; Intini, F. P.; Maresca, L.; Natile, G.; Lanfranchi, M.; Tiripicchio, A. *J. Chem. Soc., Dalton Trans.* **1991**, 1007–1015.
(55) Mao, J.-G.; Jin, Z.-S.; Ni, J.-Z. *Chin. J. Struct. Chem.* **1994**, *13*, 377–381.
(56) Berthet, J. C.; Nierlich, M.; Ephritikhine, M. *Chem. Commun.* **2003**, 1660–1661.
(57) Berthet, J. C.; Nierlich, M.; Ephritikhine, M. *Dalton Trans.* **2004**, 2814–2821.
(58) Malthete, J.; Nguyen, H. T.; Destrade, C. *Liq. Cryst.* **1993**, *13*, 171–187.
(59) Nguyen, H. T.; Destrade, C.; Malthête, J. *Adv. Mater.* **1997**, *9*, 375–388.
(60) Nguyen, H. T.; Destrade, C.; Malthête, J. Phasmids and Polycatenar Mesogens. In *Handbook of Liquid Crystals*; Demus, D., Goodby, J. W., Gray, G. W., Spiess, H.-W., Vill, V., Eds.; Wiley-VCH: Weinheim, Germany, 1998; pp 865–886.

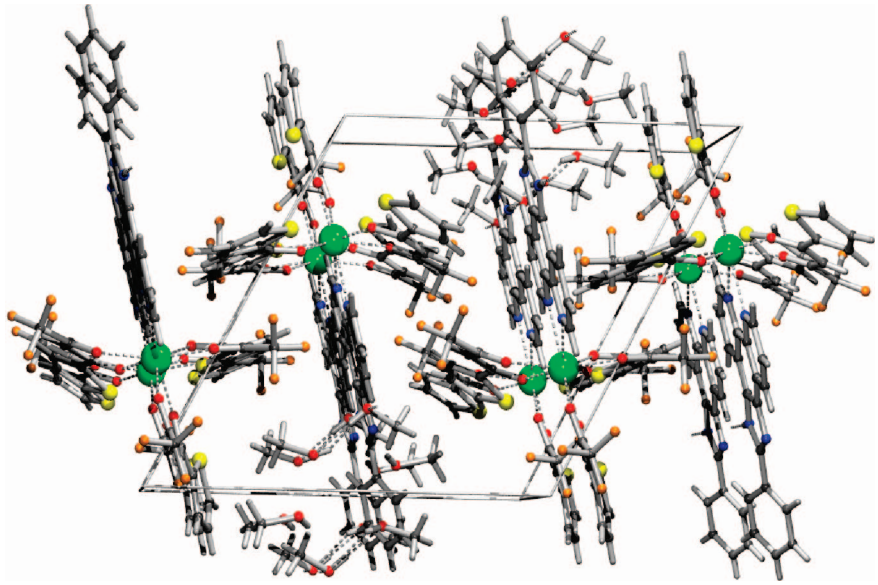

Figure 10. Packing in the crystal structure of the europium(III) complex $[Eu(tta)_3L_{XIII}]\cdot MeOH$.

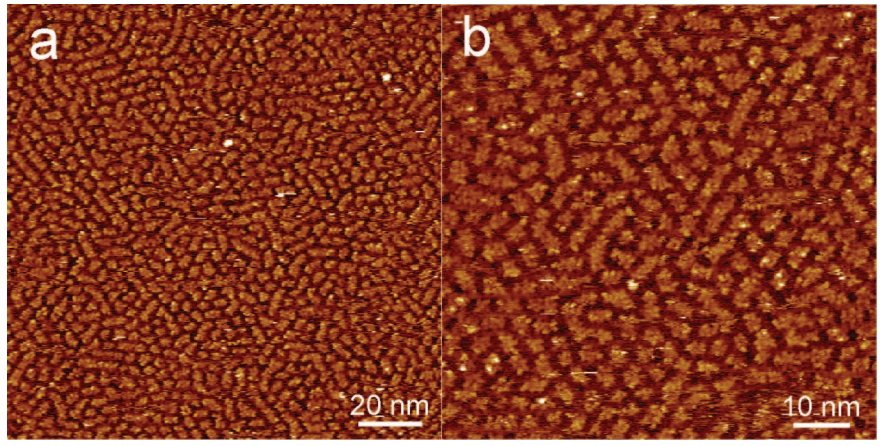

Figure 11. STM images of a self-assembled monolayer of $EuCl_3(L_{XI})_2(H_2O)$ at the graphite−1-phenyloctane interface. The bias voltage was –1.04 V, and the setpoint tunneling current was 258 pA.

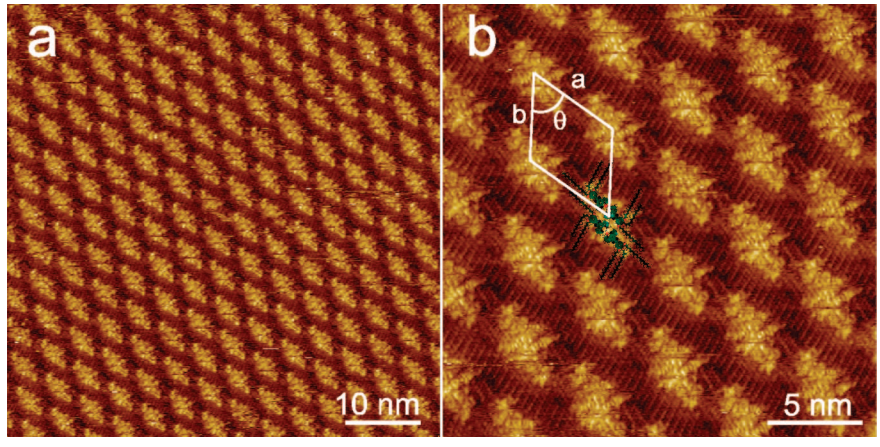

Figure 12. STM images of a self-assembled monolayer of $EuCl_3(L_{XI})_2(H_2O)$ at the graphite−octanoic acid interface. In the right-hand image, a unit cell has been marked, and a tentative molecular model of the dimer structure is shown on top of the STM image. The bias voltage was –1.04 V, and the setpoint tunneling current was 258 pA.

The most striking feature of these results was the influence of water molecules on the thermal behavior of the ligands. As mentioned above, all of the ligands contained 0.5 equiv of water, which led to the formation of dimers. To examine the influence of solvent molecules, L_{VI} was recrystallized from ethanol. After the compound was (insufficiently) dried under reduced pressure, a 1:2 water adduct $L_{VI}\cdot 2H_2O$ was obtained. ^1H NMR spectroscopy confirmed the presence of water and not ethanol; the amount of water was determined by CHN analysis. The presence of water molecules changed

Table 1. Transition Temperatures and Phase Behavior of the Imidazo[4,5-*f*]-1,10-phenanthroline Ligands

ligand	phases[a] and transition temperature(s) (°C)
L_I	Cr 162 I
L_{II}	Cr 345 I
L_{III}	g 91 I
L_{IV}	g 60 I
L_V	g 64 I
L_{VI}	Cr 113 I
$L_{VI}\cdot 2H_2O$	Cr 135 Col_h 140 SmX 190 I
L_{VII}	Cr 116 I
L_{VIII}	Cr 158 I
L_{IX}	Cr 77 I
L_X	Cr 81 I
L_{XI}	Cr 83 I
L_{XII}	Cr 122 I

[a] Abbreviations: Cr = crystalline or partially crystalline phase; g = glass; Col_h = hexagonal columnar phase; SmX = disordered smectic phase (SmA or SmC); I = isotropic liquid.

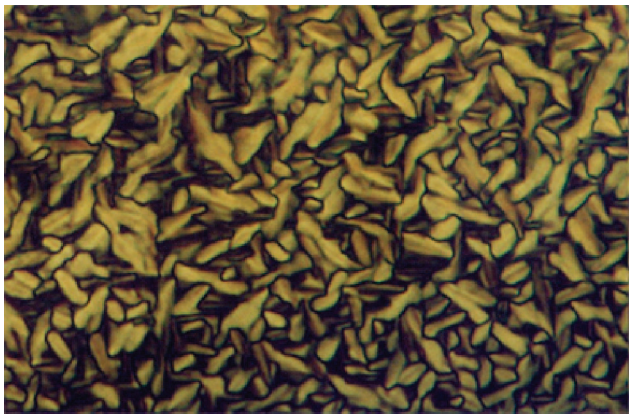

Figure 13. Optical texture of the smectic phase of $L_{VI}\cdot 2H_2O$ at 160 °C (500× magnification).

the thermal behavior of L_{VI} dramatically. Ligand L_{VI} was not liquid-crystalline, whereas the 1:2 water adduct showed two liquid-crystal phases, as first confirmed by POM, which revealed clear changes of the optical texture of the sample on heating between the lower- and higher-temperature mesophases. XRD analysis identified these two mesophases as a hexagonal columnar (Col_h) phase and a smectic phase, respectively. Figure 13 shows the texture obtained for the smectic mesophase, which precedes the isotropic liquid phase. At 135 °C, in the small-angle region of the X-ray pattern, seven sharp reflections were observed, having reciprocal spacings in a $1:\sqrt{3}:2:\sqrt{7}:3:\sqrt{12}:\sqrt{13}$ ratio. They were indexed as the hk = 10, 11, 20, 21, 30, 22, and 31 reflections, respectively, of a 2D hexagonal lattice with a lattice parameter a = 52.9 Å. In addition, a broad scattering halo was observed at 4.6 Å, corresponding to the liquidlike order of the molten aliphatic chains, and another weak halo was seen at 8.0 Å, which likely corresponded to an alternating stacking periodicity along the columnar axis (see below). At 140 °C, two additional sharp small-angle reflections in a 1:2 ratio were observed. After analysis of their profiles, it appeared that these two reflections belonged to another family of planes different from those of the Col_h phase and consequently were associated with another mesophase that coexisted with the Col_h phase; this phenomenon is rare in low-molar systems but not unusual in macromolecular materials and may be due to viscosity-induced

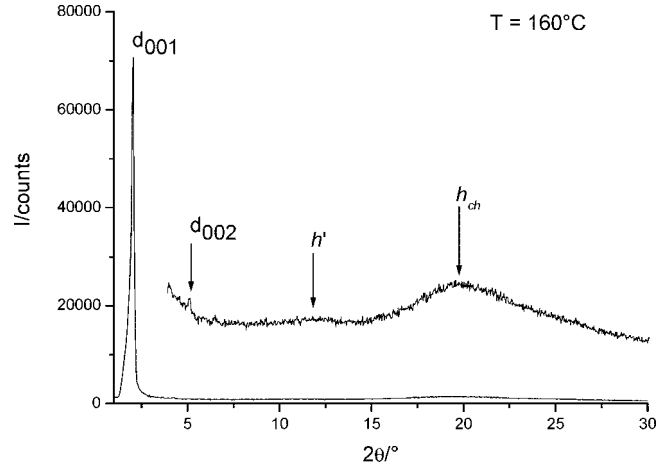

Figure 14. X-ray diffraction pattern of $L_{VI}\cdot 2H_2O$ in the smectic phase at 160 °C.

slowness of the phase-transformation kinetics. At 160 °C, only the two sharp reflections in a 1:2 ratio were observed (Figure 14). They were indicative of a lamellar structure and indexed as the 001 and 002 reflections, respectively. As above, the signal at 4.6 Å (h_{ch}) corresponded to the liquidlike order of the molten aliphatic chains, whereas the signal at 8.0 Å (h') likely was associated with the formation of supramolecular pairs or dimers, reminiscent of those in the crystalline and Col_h phases. It should be mentioned that the hexagonal columnar phase was transient and existed over a temperature range of only a few degrees. Once the smectic phase was formed at higher temperatures, the hexagonal columnar phase was not re-formed upon cooling on the time scale of the experiment.

Such an antiparallel pairing of the molecules within the smectic phase was confirmed simply by evaluating the molecular area (and supported by the cystal structure of L_I shown in Figures 2 and 3). Indeed, the value of the molecular area, A_M = 36.36 Å^2, which was obtained by dividing the molecular volume (estimated to be 1500 Å^3) by the layer periodicity (d = 41.25 Å), was too small and not compatible with the cross-sectional area of two aliphatic chains [$\sigma(CH_2) = 20.915 + 0.01593T \sim 23.45$ Å^2 per chain]. Thus, a head-to-head arrangement of the molecules in the lamellar structure ($2 \times A_M$ = 72.72 Å^2) is more likely than a head-to-tail order in a monolayer. Obviously, partial interdigitation of the chains between successive sublayers and tilting of the cores with respect to the layer normal must occur in order to compensate the molecular area and enhance the arrangement stability.

In regard to the packing within the Col_h phase, approximately six or seven imidazophenanthrolines are arranged within a columnar slice 4 Å thick (see the Supporting Information). The phenanthroline segments of the molecules form the columnar core, but because of spatial constraints and enhanced intermolecular interactions, the molecules must be tilted with respect to the columnar axis (i.e., the phenanthroline segments can neither lie flat in the lattice plane nor be perpendicular to it); consequently, this molecular assembly resembles a supramolecular propeller (as for the uranyl complexes). As for the aliphatic chains, they radiate out from the rigid columnar cores. The band at 8 Å indicated

an alternating (and regular) stacking of these propellers (rotated by 30°), guaranteeing efficient space-filling packing (as for the uranyl complexes).[39]

Thermal Behavior of the Metal Complexes. *(1) Platinum(II) Complex.* The platinum(II) complex $[PtCl_2L_{XI}]$ was not liquid-crystalline and melted at high temperature.

(2) Rhenium(I) Complexes. The rhenium(I) complexes containing the bulky $[ReBr(CO)_3]$ fragment had an appreciable dipole moment due to the polar Re−Br bond (Figure 6). This dipole was expected to influence the arrangement of the molecules in the mesophase and the solid phase. Complexation with rhenium(I) led to an increase in the melting temperatures, and none of the rhenium(I) complexes were mesomorphic.

(3) Lanthanide(III) Complexes. Complexes of the ligands L_I, L_{III}, L_{IV}, L_V, L_{VII}, L_{VIII}, L_{IX}, L_X, and L_{XI} with lanthanum(III) were prepared in order to examine the influence of the substitution pattern and alkoxy chain length on the thermal behavior of the metal complexes $[LaCl_3(L)_2(H_2O)]$ (L = L_I, L_{III}, L_{IV}, L_V, L_{VII}, L_{VIII}, L_{IX}, L_X, L_{XI}). Except for the lanthanum(III) complex $[LaCl_3(L_{XI})_2(H_2O)]$, which exhibited a cubic phase (see below), none of the lanthanum(III) complexes were liquid-crystalline. Complexes of the ligands having 2,3,4- and 2,4,5-trisubstitution patterns ($[LaCl_3(L_{IX})_2(H_2O)]$ and $[LaCl_3(L_X)_2(H_2O)]$, respectively) melted directly to the isotropic liquid. Complexes of the ligands with fewer than three alkoxy chains ($[LaCl_3(L)_2(H_2O)]$, L = L_I, L_{III}, L_{IV}, L_V, L_{VII}, L_{VIII}) all decomposed before melting at temperatures above 300 °C. A comparison of the thermal behavior of the complexes $[LaCl_3(L_{IX})_2(H_2O)]$, $[LaCl_3(L_X)_2(H_2O)]$, and $[LaCl_3(L_{XI})_2(H_2O)]$ shows that the long tetradecyloxy chain at the 2-position prohibited the formation of a mesophase. The lateral alkoxy chain at the 2-position strongly reduced lateral interactions between the molecules and also reduced microsegregation.

Complexes of ligand L_{XI} with lanthanum(III), praseodymium(III), neodymium(III), samarium(III), europium(III), gadolinium(III), terbium(III), dysprosium(III), and holmium(III) were synthesized in order to study the influence of the lanthanide contraction on the thermal behavior of the metal complexes $[LnCl_3(L_{XI})_2(H_2O)]$ (Ln = La, Pr, Nd, Sm, Eu, Gd, Tb, Dy, Ho). The lanthanide contraction is the gradual decrease in the ionic radii of the trivalent lanthanide ions as one moves across the lanthanide series. The thermal behavior of the lanthanide(III) complexes is summarized in the phase diagram shown in Figure 15. As the metal ion changed from lanthanum(III) to holmium(III), there was a gradual increase in the melting temperature and a strong decrease in the clearing temperature. The La−Eu complexes formed an enantiotropic cubic mesophase, whereas the Gd−Ho complexes were not liquid-crystalline. A monotropic (cubic) mesophase was expected for the complexes of the heavy lanthanides, but because of the fast crystallization of the complexes on cooling from the isotropic liquid, such a monotropic mesophase could not be observed. Thus, the lanthanide(III) ion had a great influence on the thermodynamic stability of the mesophase, which decreased across the lanthanide series until the the liquid-crystalline properties

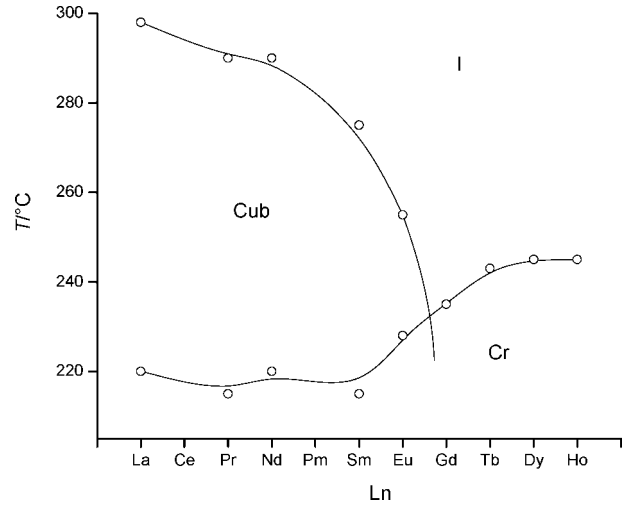

Figure 15. Phase diagram of the lanthanide(III) complexes $[LnCl_3(L_{XI})_2(H_2O)]$ (Cr = crystalline phase, Cub = cubic phase, I = isotropic liquid).

were completely lost for complexes of lanthanide(III) ions having an ionic radius smaller than that of europium(III). The strong effect of the lanthanide(III) ion on the transition temperature is in agreement with that observed for lanthanide(III) alkanoates[61] and for Schiff base complexes with nitrate counterions, for which either the mesophase stability was considerably decreased or the liquid-crystalline properties were totally suppressed as one moved across the lanthanide series from lanthanum(III) to lutetium(III).[17]

Other polycatenar lanthanidomesogens were also reported to exhibit a cubic phase having an *Im*3*m* cubic space group.[19] In these cases, the polycatenar ligands L_i possessed either a linear or a bent shape, and upon complexation with $Ln(NO_3)_3$, the corresponding nitrato complexes $[Ln(L_i)(NO_3)_3]$ adopted either a bent or a linear shape, respectively. They showed a lamellar mesophase (Ln = Pr, Nd for the bent complexes and Ln = Pr−Gd, Dy, Tm for the linear ones), an *Im*3*m* cubic phase for Ln = Pr−Ho, and a Col_h phase for Ln = Er−Lu. Thus, the mesomorphic behavior was also found to be sensitive to the lanthanide contraction, although in a more spectacular way than in the presently described lanthanidomesogens, as lamellar and cubic phases were favored for the light lanthanides as opposed to the Col_h phase induced for the heavier lanthanides. In the case of the $[LnCl_3(L_{XI})_2(H_2O)]$ complexes, the thermal stability was considerably enhanced compared with that of the $[Ln(L_i)(NO_3)_3]$ complexes.

Cubic mesophases are rather uncommonly observed in thermotropic systems and are not easy to detect and characterize.[4,6,19,62–67] No texture could be observed, only the formation of large black (optically isotropic) viscous

(61) Binnemans, K.; Jongen, L.; Görller-Walrand, C.; D'Olieslager, W.; Hinz, D.; Meyer, G. *Eur. J. Inorg. Chem.* **2000**, 1429–1436.
(62) Diele, S. *Curr. Opin. Colloid Interface Sci.* **2002**, *7*, 333–342.
(63) Imperor-Clerc, M. *Curr. Opin. Colloid Interface Sci.* **2005**, *9*, 370–376.
(64) Kutsumizu, S. *Curr. Opin. Solid State Mater. Sci.* **2002**, *6*, 537–543.
(65) Tschierske, C. *Curr. Opin. Colloid Interface Sci.* **2002**, *7*, 69–80.
(66) Diele, S.; Goring, P. Thermotropic Cubic Phases. In *Handbook of Liquid Crystals*; Demus, D., Goodby, J. W., Gray, G. W., Spiess, H.-W., Vill, V., Eds.; Wiley-VCH: Weinheim, Germany, 1998; pp 887–900.

Table 2. Bragg Reflections Collected from the X-ray Diffraction Patterns of the Cubic Lanthanide(III) Complexes

compound	d_{meas} (Å)[a]	$h^2 + k^2 + l^2$	hkl[b]	I[c]	d_{calc} (Å)[a,d]	parameters at temperature T[d]
$[LaCl_3(L_{XI})_2(H_2O)]$	41.01	4	200	S	40.89	$T = 260$ °C
	36.43	5	210	VS	36.58	$a = 81.78$ Å
	33.41	6	211	S	33.39	Cub-$Pm\bar{3}n$
	25.88	10	310	W	25.86	$N = 136.7$
	8.25			br		
	4.6			br		
$[PrCl_3(L_{XI})_2(H_2O)]$	41.15	4	200	M	41.18	$T = 240$ °C
	36.85	5	210	VS	36.83	$a = 82.36$ Å
	33.63	6	211	S	33.62	Cub-$Pm\bar{3}n$
	8.3			br		$N = 139.7$
	4.6			br		
$[NdCl_3(L_{XI})_2(H_2O)]$	41.19	4	200	M	41.07	$T = 240$ °C
	36.68	5	210	VS	36.73	$a = 82.14$ Å
	33.49	6	211	S	33.53	Cub-$Pm\bar{3}n$
	8.25			br		$N = 138.5$
	4.6			br		
$[SmCl_3(L_{XI})_2(H_2O)]$	40.12	4	200	S	40.0	$T = 220$ °C
	35.66	5	210	VS	35.78	$a = 80.0$ Å
	32.65	6	211	S	32.66	Cub-$Pm\bar{3}n$
	8.25			br		$N = 128$
	4.6			br		
$[EuCl_3(L_{XI})_2(H_2O)]$	39.9	4	200	W	39.62	$T = 230$ °C
	35.42	5	210	VS	35.44	$a = 79.25$ Å
	32.14	6	211	VS	32.35	Cub-$Pm\bar{3}n$
	8.38			br		$N = 124.5$
	4.7			br		

[a] d_{meas} and d_{calc} are the measured and calculated diffraction spacings, respectively. [b] hkl are the indices of the reflection. [c] I is the intensity of the reflection: VS, very strong; S, strong; M, medium. The abbreviation br stands for broad reflection. [d] d_{calc} ($=\langle d_{hkl}\rangle$) and the lattice parameter a were deduced from the following mathematical expressions: $a = [\Sigma d_{hkl}(h^2 + k^2 + l^2)^{1/2}]/N_{hkl}$, where N_{hkl} is the number of hkl reflections, and $\langle d_{hkl}\rangle = a/(h^2 + k^2 + l^2)^{1/2}$. N is the number of molecules per cubic cell: $N = a^3/V_{mol}$, where $V_{mol} \approx 4000$ Å^3.

areas. They were distinguished from the corresponding isotropic liquids by their higher viscosities and often by the faceting of air bubbles having distorted polygonal shapes entrapped in the sample. In other cases, applying some pressure with a spatula on the coverslip induced flashes of light, which immediately disappeared when the pressure was released. However, no precise structural information could be deduced from this technique only, and unequivocal mesophase assignment was achieved by X-ray diffraction. The Bragg reflections collected from the X-ray diffraction patterns of the cubic mesophases of all of the lanthanide(III) complexes are listed in Table 2.

The cubic structure of each of these mesophases was deduced from a set of four or three sharp small-angle reflections for which the reciprocal spacings were in a $\sqrt{4}$:$\sqrt{5}$:$\sqrt{6}$:$\sqrt{10}$ (Ln = La) or $\sqrt{4}$:$\sqrt{5}$:$\sqrt{6}$ (Ln = Pr, Nd, Sm, Eu) ratio (Table 2), although with such a small number of reflections, the determination of the cubic space group was very difficult. Along with these sharp reflections, two broad scattering features were observed, a weak one at 8.2–8.4 Å and a strong one at 4.6–4.7 Å, corresponding to some weak intermolecular correlations and molten aliphatic chains, respectively. Nevertheless, these reflections were indexed as the 200, 210, 211, and 310 reflections of a primitive cubic cell on the basis of the following analysis. For a body-centered (*I*-type) cubic lattice, the considered ratios in this case would be $\sqrt{8}$:$\sqrt{10}$:$\sqrt{12}$:$\sqrt{20}$ for Ln = La and $\sqrt{8}$:$\sqrt{10}$:$\sqrt{12}$ for Ln = Pr, Nd, Sm, Eu (the general condition for the hkl reflections is $h + k + l = 2n$), all compatible with this symmetry. These reflections could then be indexed as 220, 310, 222, and 420. However, quite a large number of reflections (7) were missing, and not all of these absences were explained by the reflection conditions (the only absence so explained was the 200 reflection in the $I4_132$ group). Among the 10 body-centered space groups, $Ia\bar{3}$ and $Ia\bar{3}d$ were excluded because of the presence of the 310 reflection, and $I\bar{4}3d$ was excluded because of the 222 reflection, leaving seven possible but unlikely space groups ($I23$, $I2_13$, $Im\bar{3}$, $I432$, $I4_132$, $I\bar{4}3m$, and $Im\bar{3}m$). In the case of a face-centered (*F*-type) space group, the compatible reflection ratio $\sqrt{16}$:$\sqrt{20}$:$\sqrt{24}$:$\sqrt{40}$ (with conditions $h + k$, $h + l$, $k + l = 2n$) would allow the reflections to be indexed as 400, 420, 422, and 620. The presence of $\sqrt{20}$ automatically excluded the diamond structure. Only six of 11 face-centered space groups were compatible ($F23$, $Fm\bar{3}$, $F432$, $F4_132$, $F\bar{4}3m$, and $Fm\bar{3}m$). However, the 10 intermediate reflections that were missing and could not be explained by the reflection conditions of these six space groups ($k, l = 2n$ for $0kl$, $h = 2n$ for $h00$, and $h + l = 2n$ for hhl) did not favor the assignment of a face-centered space group. As far as the 15 primitive (*P*-type) cubic space groups were concerned, several could be immediately disregarded because of the presence of some particular reflections, such as the 200 reflection (which excluded $P4_332$ and $P4_132$), the 210 reflection (which excluded $Pn\bar{3}$, $Pn\bar{3}n$, and $Pn\bar{3}m$), and the 310 reflection (which excluded $Pa\bar{3}$). Among the nine remaining primitive space groups, the most probable ones were $Pm\bar{3}n$ and $P\bar{4}3n$, since three of the five absent reflections, namely 100, 300, and 221, were explained by the space-group conditions ($h = 2n$ for $h00$ and $l = 2n$ for hhl); the least probable space groups were $P2_13$ and $P4_232$ ($h = 2n$ for $h00$) and $P23$, $Pm\bar{3}$, $P432$, $P\bar{4}3m$, and $Pm\bar{3}m$

(67) Fazio, D.; Mongin, C.; Donnio, B.; Galerne, Y.; Guillon, D.; Bruce, D. W. *J. Mater. Chem.* **2001**, *11*, 2852–2863.

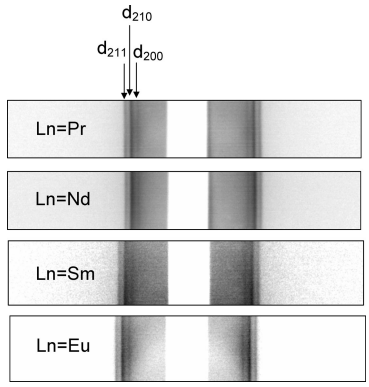

Figure 16. Small-angle X-ray patterns of four of the lanthanide(III) complexes $[LnCl_3(L_{XI})_2(H_2O)]$, recorded at 240 °C (Ln = Pr, Nd), 230 °C (Ln = Sm), and 220 °C (Ln = Eu).

(no conditions). None of the space groups retained in this list have yet been found for a liquid-crystalline cubic phase, except for the $Pm\bar{3}n$ cubic space group (No. 223).[62–64]

Thus, we were left with nine primitive, seven body-centered, and six face-centered (the least probable) space groups. An interesting piece of evidence for considering primitive rather than body-centered space groups was the distribution of the intensity of the reflections in the XRD pattern as a function of the diffraction angle. In essentially all of the reported body-centered cubic structures,[62–66] the intensity decreased progressively with increasing diffraction angle in the corresponding X-ray patterns, but this was not the case for primitive cubic cells.[68] Here, we did not observe this progressive decrease of reflection intensity with increasing diffraction angle (Figure 16): the strongest reflection, 210, was always found between the 200 and 211 reflections. From these simple arguments (distribution of reflection intensities, reflection absences unexplained by the space-group conditions), both the body-centered and face-centered symmetries were excluded, and thus we assigned the most probable primitive cubic space group, $Pm\bar{3}n$, as the space group of the mesophases.

Recently, a model for the $Pm\bar{3}n$ cubic phase, intermediate between micellar and bicontinuous topologies, was suggested and found to give a fair account of the organization of semirigid dendrimers within this mesophase (Figure 17).[68] Such a model can be fully applied here and consists of the formation of an infinite 3D interlocking network of mutually perpendicular, evenly pinched columns, compatible with the symmetry of the space group [three pairs of column sites evenly spaced along the bisectors of the cubic cell faces and two interstitial sites at the center and corners of the cubic lattice (Figure 17; also see the Supporting Information). This model imposes some constraints on the molecular disposition, as evidenced by the broad band at 8.2–8.4 Å.

(4) Summary. An overview of the transition temperatures and phase behavior of all of the metal complexes is given in Table 3. It is somewhat surprising that many of the metal complexes were not liquid-crystalline. However, upon complexation with rhenium(I), platinum(II), and europium(III) ($[Eu(tta)_3L_{XIII}]$ complex), a bulky metal fragment was introduced. Siting the bulky metal fragment at one extremity of the molecule precluded the formation of a mesophase. This was also observed for the ortho-metallated imine complexes of rhenium(I) prepared by Bruce and co-workers,[69] where the introduction of the bulky rhenium(I) fragment at one end of the molecule destabilized but did not suppress the mesomorphism. For metal complexes with a higher metal-to-ligand ratio, such as the lanthanide(III) complexes of ligand L_{XI} with a 1:2 metal-to-ligand ratio and the uranyl complex with a 1:3 metal-to-ligand ratio, mesophases with a broad temperature range were observed. This

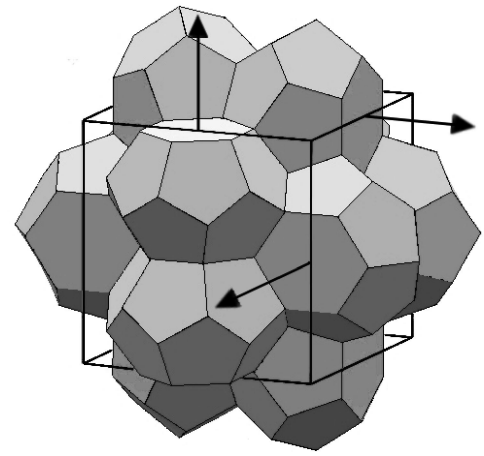

Figure 17. Schematic representation of the model lattice consisting of 3D interlocking pinched columns. The arrows indicate the growth directions of the evenly pinched columns.

Table 3. Transition Temperatures and Phase Behavior of the Metal Complexes

compound	phases[a] and transition temperature(s) (°C)
$[PtCl_2L_{XI}]$	Cr 195 I
$[ReBr(CO)_3L_{II}]$	Cr 371 I
$[ReBr(CO)_3L_{III}]$	Cr 244 I
$[ReBr(CO)_3L_{IV}]$	Cr 216 I
$[ReBr(CO)_3L_{V}]$	Cr 197 I
$[ReBr(CO)_3L_{VII}]$	Cr 183 I
$[ReBr(CO)_3L_{VIII}]$	Cr 92 I
$[ReBr(CO)_3L_{IX}]$	Cr 178 I
$[ReBr(CO)_3L_{X}]$	Cr 180 I
$[ReBr(CO)_3L_{XI}]$	Cr 91 I
$[LaCl_3(L_I)_2(H_2O)]$	Cr dec >300
$[LaCl_3(L_{III})_2(H_2O)]$	Cr dec >300
$[LaCl_3(L_{IV})_2(H_2O)]$	Cr dec >300
$[LaCl_3(L_{V})_2(H_2O)]$	Cr dec >300
$[LaCl_3(L_{VII})_2(H_2O)]$	Cr dec >300
$[LaCl_3(L_{VIII})_2(H_2O)]$	Cr dec >300
$[LaCl_3(L_{IX})_2(H_2O)]$	Cr 234 I
$[LaCl_3(L_{X})_2(H_2O)]$	Cr 242 I
$[LaCl_3(L_{XI})_2(H_2O)]$	Cr 220 Cub 298 I
$[PrCl_3(L_{XI})_2(H_2O)]$	Cr 215 Cub 290 I
$[NdCl_3(L_{XI})_2(H_2O)]$	Cr 220 Cub 290 I
$[SmCl_3(L_{XI})_2(H_2O)]$	Cr 215 Cub 275 I
$[EuCl_3(L_{XI})_2(H_2O)]$	Cr 228 Cub 255 I
$[GdCl_3(L_{XI})_2(H_2O)]$	Cr 235 I
$[TbCl_3(L_{XI})_2(H_2O)]$	Cr 243 I
$[DyCl_3(L_{XI})_2(H_2O)]$	Cr 245 I
$[HoCl_3(L_{XI})_2(H_2O)]$	Cr 245 I
$[UO_2(L_{XI})_3](CF_3SO_3)_2$	Cr 95 Col_h 181 I

[a] Abbreviations: Cr = crystalline or semi or partially crystalline phase; Col_h = hexagonal columnar phase; Cub = cubic phase; I = isotropic liquid; dec = decomposition.

(68) Bury, I.; Heinrich, B.; Bourgogne, C.; Guillon, D.; Donnio, B. *Chem.—Eur. J.* **2006**, *12*, 8396–8413.

(69) Guillevic, M. A.; Danks, M. J.; Harries, S. K.; Collinson, S. R.; Pidwell, A. D.; Bruce, D. W. *Polyhedron* **2000**, *19*, 249–257.

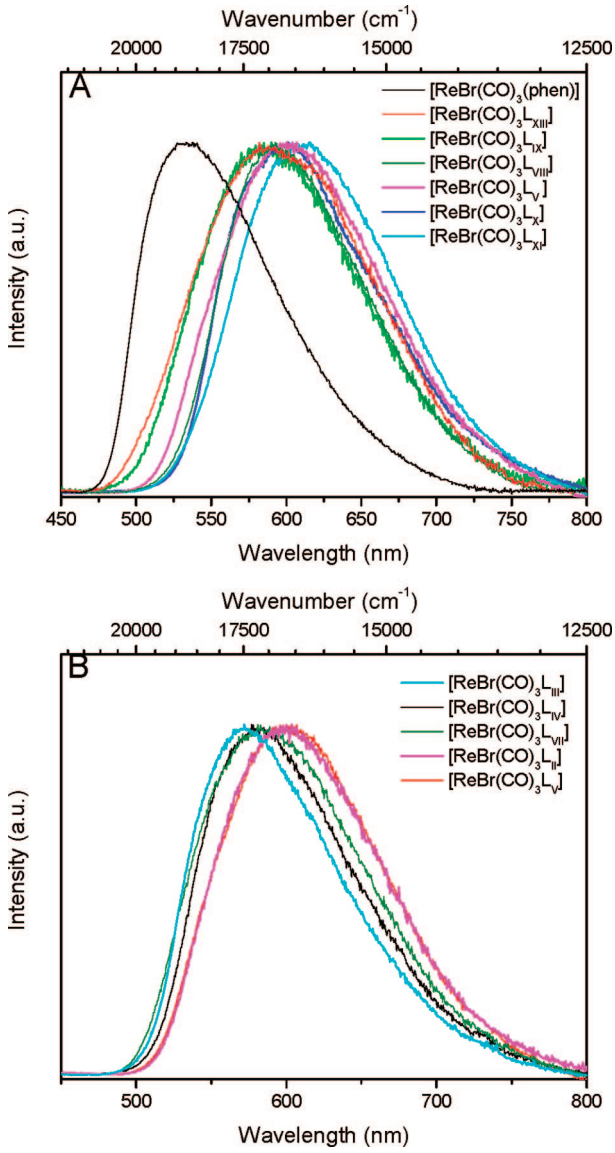

Figure 18. Normalized emission spectra for rhenium(I) imidazo[4,5-*f*]-1,10-phenanthroline and rhenium(I) 1,10-phenanthroline powders between two glass plates at room temperature (L_{XIII} is phenylimidazo[4,5-*f*]-1,10-phenanthroline). The influences of (A) the substitution pattern and (B) the length of the alkyl chains are shown. The excitation wavelength was 350 nm.

can be attributed to the higher number of ligands that coordinate to the metal ion, to the geometry of these complexes, and, in the case of the uranyl complex, to its ionic character.[16] In the uranyl complex, the uranyl ion acts as a template to bring the ligands into the correct position, so that the propeller-like units can arrange into columns. These metallomesogens stack in such a way that the polar order is annihilated.

Photophysical Properties. It is well known that rhenium(I) tricarbonyl halide complexes containing a bidentate α-diimine ligand can display intense photoluminescence in the visible spectral region.[70] Normalized luminescence spectra for powdered samples of the rhenium(I) complexes between two glass plates are shown in Figure 18. All of the rhenium(I) tricarbonyl halide complexes with an imidazo[4,5-*f*]-1,10-phenanthroline ligand emitted yellowish light. The broad emission band had a maximum around 590 nm. The luminescence band was red-shifted in comparison with the emission band of the analogous complex with 1,10-phenanthroline [$ReBr(CO)_3$(phen)]. The imidazo[4,5-*f*]-1,10-phenanthroline ligand possesses a more delocalized π system, which lowers the energy of the intraligand excited state. The character of the lowest excited state of tricarbonyl halide complexes [$ReX(CO)_3$(α-diimine)] can change from metal-to-ligand charge transfer (MLCT) for X = Cl to ligand-to-ligand charge transfer (LLCT) for X = I.[71] The complexes with X = Br have an intermediate character. The emission maximum and the shape of the emission band changed slightly when the positions and lengths of the alkyl-chain substituents were altered, but it was difficult to find a systematic trend. The influence of methyl substituents of 1,10-phenanthroline on the emission spectra of the [$ReCl(CO)_3$(phen)] and [$Re(CO)_3$(phen)(pyridine)]$^+$ complexes was described previously.[72,73]

The trivalent lanthanide ions are also well-known for their luminescence properties.[74] Because of the low molar absorptivities (<10 L mol^{-1} cm^{-1}) of f−f transitions, it is difficult to efficiently excite the lanthanide ions directly in the 4f levels, so the so-called "antenna effect" is used to increase the luminescence intensity. The antenna effect is based on strong light absorption by organic ligands surrounding the lanthanide ions and on the subsequent transfer of the excitation energy from the ligand triplet state to the 4f levels of the lanthanide ion. β-Diketonates are excellent ligands for lanthanides because of the formation of six-membered chelate rings.[75] The binding of three β-diketonate ligands to the lanthanide ion leaves enough space around the ion for the binding of two additional water molecules, so that the lanthanide ion can expand its coordination number to 8. These water molecules can easily deactivate the excited states of the lanthanide ion and thus partially or totally quench the photoluminescence. However, the water molecules can be expelled from the lanthanide ion by reaction with a bidentate ligand such as 1,10-phenanthroline. The resulting Lewis base adduct of the lanthanide tris(β-diketonate) complex has a higher luminescence efficiency than the hydrated lanthanide tris(β-diketonate) complex. The normalized luminescence spectra for the europium(III) complexes with tta or dibenzoylmethanate (dbm) and imidazo[4,5-*f*]-1,10-phenanthroline are shown in Figure 19. Excitation was done at 350 nm in the β-diketonate ligands. The europium(III), neodymium(III), and samarium(III) imidazo[4,5-*f*]-1,10-phenanthroline chloro complexes [$LnCl_3(L_{XI})_2(H_2O)$] showed only a very weak luminescence. Two reasons for this behavior can be given. First, the triplet levels of L_{XI} were not as well positioned as those of the β-diketonates to excite the europium(III) levels. Second, the chloro complexes had a water molecule directly attached to the lanthanide ion,

(70) Sacksteder, L.; Zipp, A. P.; Brown, E. A.; Streich, J.; Demas, J. N.; Degraff, B. A. *Inorg. Chem.* **1990**, *29*, 4335–4340.
(71) Stufkens, D. J.; Vlcek, A. *Coord. Chem. Rev.* **1998**, *177*, 127–179.
(72) Striplin, D. R.; Crosby, G. A. *Coord. Chem. Rev.* **2001**, *211*, 163–175.
(73) Wallace, L.; Rillema, D. P. *Inorg. Chem.* **1993**, *32*, 3836–3843.
(74) Bünzli, J. C. G.; Piguet, C. *Chem. Soc. Rev.* **2005**, *34*, 1048–1077.
(75) Binnemans, K. Rare-Earth β-Diketonates. In *Handbook on the Physics and Chemistry of Rare Earths*; Gschneidner, K. A., Bünzli, J. C. G., Pecharsky, V. K., Eds.; Elsevier: Amsterdam, 2005; pp 107–272.

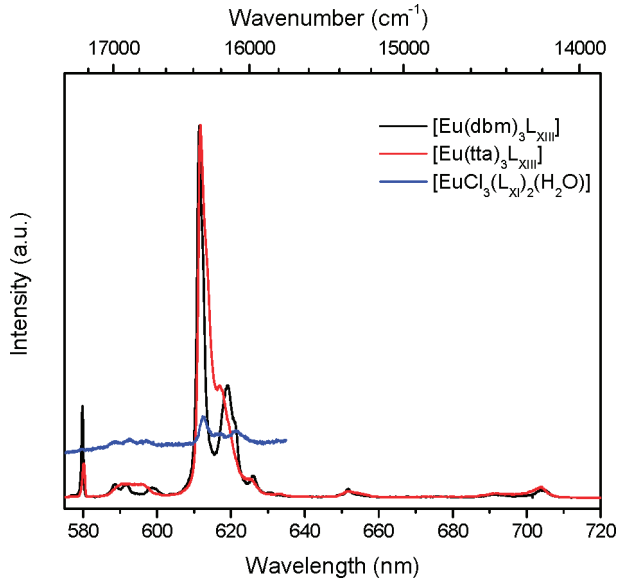

Figure 19. Normalized emission spectra at room temperature for powders of the europium(III) imidazo[4,5-*f*]-1,10-phenanthroline tta, dbm, and chloro complexes. The excitation wavelength was 350 nm.

and this water could easily quench the luminescence. The luminescence spectrum for the europium(III) chloro complex is also shown in Figure 19.

Conclusions

Transformation of 1,10-phenanthroline into substituted 2-arylimidazo[4,5-*f*]-1,10phenanthroline via condensation of 1,10-phenanthroline-5,6-dione with a substituted benzaldehyde in the presence of ammonium acetate is a facile route to functionalize 1,10-phenanthrolines. By a proper choice of the substitution pattern of the substituted benzaldehydes, it is possible to obtain lipophilic 1,10-phenanthroline ligands, which are useful for the design of metallomesogens. Depending on the nature of the metal ion, complexes with 1:1, 1:2, or 1:3 metal-to-ligand ratios are possible, and these structural variations lead to a modification of the thermal behavior. More specifically, the easy access to variously substituted ligands and the fact that these ligands can form complexes with a wide variety of metal ions provide the opportunity to tune the mesophase behavior by altering the space-filling abilities (and thus the packing constraints) via the complex geometry and/or the substitution pattern and chain length. In the present work, although the ligands were not liquid-crystalline, some of the metal complexes showed a mesophase over a broad temperature range. The most stable mesophases were observed for the lanthanide(III) complexes of ligand L_{XI} and the uranyl complex, for which the metal-to-ligand ratios were 1:2 and 1:3, respectively. The enhanced mesophase stability of these complexes was due to the higher number of ligands, which resulted in a different geometry, although it is interesting to point out the ionic character of the uranyl complex. The $EuCl_3(L_{XI})_2(H_2O)$ complex formed self-assembled monolayers at the graphite−solution interface. An STM study indicated that the order of these monolayers strongly depended on the solvent. Whereas rather disordered monolayers were obtained at the graphite−1-phenyloctane interface, well-ordered monolayers were observed at the graphite−octanoic acid interface. All of the rhenium(I) complexes showed a yellow photoluminescence. Europium(III) complexes with tta or dbm and imidazo[4,5-*f*]-1,10-phenanthroline showed an intense red photoluminescence, whereas lanthanide(III) complexes of the type $[LnCl_3(L_{XI})_2(H_2O)]$ (Ln = Nd, Sm, Eu) showed only a very weak photoluminescence.

Acknowledgment. T.C. and K.D. thank the FWO-Flanders for a postdoctoral fellowship. D.G. and B.D. thank CNRS and ULP for support and funding and Dr. C. Bourgogne for the geometrical representations of the cubic phase. K.B. thanks the K.U. Leuven (Projects GOA 03/03 and IDO/05/005) and the FWO-Flanders (Project G.0508.07). Funding for travel was obtained via a Tournesol project (Project T2004.10) and via the COST ACTION D35 (Working Group D35/0004/05). The authors acknowledge Prof. Dr. Suzanne Toppet for assistance with the NMR measurements and for useful discussions. Mass spectra were measured by Leen Van Nerum and Bert Demarsin. CHN analyses were performed by Petra Bloemen and Dirk Henot.

Supporting Information Available: Synthetic procedures and characterization data, NMR spectra, XRD data, and geometrical representations of the 3D interlocking pinched columns model (PDF). Crystallographic information for the crystal structures (CIF). This material is available free of charge via the Internet at http://pubs.acs.org. CCDC-606328, -606329, and -606330 contain the supplementary crystallographic data for this paper and can be obtained free of charge via www.ccdc.cam.ac.uk/conts/retrieving.html or from the Cambridge Crystallographic Data Centre, 12 Union Road, Cambridge CB2 1EZ, U.K. (fax, +44–1223–336033; e-mail, deposit@ccdc.cam.ac.uk).

CM070637I